Sea-level variability and change along the Norwegian coast between 2003 and 2018 from satellite altimetry, tide gauges and hydrography

Fabio Mangini[1], Léon Chafik[2], Antonio Bonaduce[1], Laurent Bertino[1], Jan Even Ø. Nilsen[3]

[1]Nansen Environmental and Remote Sensing Center and Bjerknes Centre for Climate Research, Bergen, Norway
[2]Department of Meteorology and Bolin Centre for Climate Research, Stockholm, Sweden
[3]Institute of Marine Research and Bjerknes Centre for Climate Research, Bergen, Norway

Correspondence to: Fabio Mangini (fabio.mangini@nersc.no)

Abstract. Sea-level variations in coastal areas can differ significantly from those in the nearby open ocean. Monitoring coastal sea-level variations is therefore crucial to understand how climate variability can affect the densely populated coastal regions of the globe. In this paper, we study the sea-level variability along the coast of Norway by means of in situ records, satellite altimetry data, and a network of eight hydrographic stations over a period spanning 16 years (from 2003 to 2018). At first, we evaluate the performance of the ALES-reprocessed coastal altimetry dataset by comparing it with the sea-level anomaly from tide gauges over a range of timescales, which include the long-term trend, the annual cycle and the detrended and deseasoned sea level anomaly. We find that coastal altimetry outperforms conventional altimetry products at most locations along the Norwegian coast. We later ~~take advantage of the coastal altimetry dataset to~~ perform a sea level budget along the Norwegian coast. We find that the thermosteric and the halosteric signals give a comparable contribution to the sea-level trend along the Norwegian coast, except for three, non-adjacent hydrographic stations, where salinity variations affect the sea-level trend more than temperature variations. We also find that the sea-level annual cycle is more affected by variations in temperature than in salinity, and that both temperature and salinity give a comparable contribution to the detrended and deseasoned sea-level along the entire Norwegian coast.

1 Introduction

Sea-level is considered a key indicator to monitor the earth's energy imbalance and climate change (e.g., Oppenheimer et al., 2019; von Schuckmann et al., 2018). An accurate estimate of sea-level rise is one of the major challenges of climate research (e.g., Eyring et al., 2016) with large societal benefit and impact due to the large human population living in coastal areas (e.g., Lichter et al., 2011). The Norwegian coast is no exception. While it appears little vulnerable to sea-level variations because of its steep topography and rocks resistant to erosion, it has a large number of coastal cities, most of which have undergone significant urban development in recent times (Simpson et al., 2015).

29 Since August 1992, when NASA and CNES launched the TOPEX/Poseidon mission, satellite altimetry has enormously

30 expanded our knowledge of the ocean and the climate system (e.g., Cazenave et al., 2018). With the help of satellite

31 altimetry, oceanographers and climate scientists could observe sea-level variations over almost the entire ocean (e.g., Nerem

32 et al., 2010; Madsen et al., 2019) and understand their causes (e.g., Richter et al., 2020), detect ocean currents (e.g., Zhang et

33 al., 2007) and monitor their variability (e.g., Chafik et al., 2015), observe the evolution of climate events (e.g., Ji et al., 2000)

34 and investigate their origins (e.g., Picaut et al., 2002). Satellite altimetry has made these, and other achievements, possible

35 because it has provided continuous sea-level observations over large parts of the ocean, in areas where sea-level

36 measurements were previously only occasional.

37

38 While invaluable over the open ocean, satellite altimetry measurements have historically been flagged as unreliable within

39 20-50 km from the coast (e.g., Benveniste et al., 2020). Indeed, the accuracy of radar altimetry, which is 2-3 cm over the

40 open ocean (e.g., Volkov and Pujol, 2012), deteriorates in coastal regions because of technical issues (e.g., Xu et al., 2019).

41 Notably, land contaminates the returned echoes of radar altimeters, and the complex topography of continental shelves,

42 together with the irregular shape of most coastlines, makes geophysical corrections in coastal areas less accurate than in the

43 open ocean.

44

45 To increase the accuracy of radar altimetry in coastal regions, Passaro et al. (2014) have developed the Adaptive Leading

46 Edge Subwaveform (ALES) retracking algorithm. The ALES retracker addresses the altimeter footprint contamination issue

47 by avoiding echoes from bright targets (e.g., land). Several studies have found a clear improvement of the ALES-reprocessed

48 satellite altimetry observations over conventional altimetry products in different areas of the World (e.g., Passaro et al.,

49 2014, 2015, 2016, 2018, 2021), with the new algorithm providing estimates of the altimetry parameters in coastal areas with

50 levels of accuracy typical of the open ocean (e.g., Passaro et al., 2014).

51

52 In this paper, we investigate how the ALES-reprocessed satellite altimetry dataset resolves sea-level along the coast of

53 Norway compared to all the tide-gauge records available over the 16-year period between 2003 and 2018. Indeed, to the best

54 of our knowledge, previous validation studies have not considered the entire Norwegian coast, but only parts of it: Passaro et

55 al. (2015) focused on the transition zone between the North Sea and the Baltic Sea, whereas Rose et al. (2019) focused on

56 Honningsvåg, in northern Norway. The Norwegian coast also appears particularly interesting for validation purposes

57 because, during the altimetry period, it is well covered by tide gauges, and because conventional altimetry products have

58 previously failed to reproduce the sea-level trends in the region (Breili et al., 2017). The present study will thus investigate

59 the performance of ALES in relation to these issues.

60

61 We further use the ALES-reprocessed altimetry dataset in combination with a network of hydrographic stations along the

62 coast of Norway to study the local sea-level budget, which is known to be challenging at the regional scale (e.g., Raj et al.,

63 2020; Richter et al., 2012). Richter et al. (2012) have already used tide gauges and hydrographic stations to assess the

64 different contributions to the Norwegian sea-level variability between 1960 and 2010. However, compared to their study, we

65 use the coastal altimetry dataset to reconstruct a monthly mean sea level time series centred over each hydrographic station.

66 This is an advantage over Richter et al. (2012) since the tide gauges and the hydrographic stations can be as far as 100 km

67 apart. Moreover, compared to Richter et al. (2012), we analyse the annual cycle of the sea-level more in detail by describing

68 how its properties change along the Norwegian coast.

69

70 This paper is organized as follows. Section 2 describes the data used in the coastal sea-level signal analysis. An analysis of

71 sea-level components retrieved by each observational instrument is provided in Section 3. The coastal sea level from tide

72 gauges and satellite altimetry are compared in terms of temporal variability and trends in Section 4. Section 5 focuses on the

73 sea-level budget combining sea-level estimates from altimetry and hydrographic data. Section 6 summarizes and concludes.

74

75 **2 Data**

76 **2.1 ALES-reprocessed multi-mission satellite altimetry**

77 To provide more accurate sea-level estimates in coastal regions, the ALES retracker operates in two stages. At first, it fits the

78 leading edge of the waveform to have a rough estimate of the significant wave height (SWH). Then, depending on the SWH,

79 the algorithm selects a portion of the waveform (known as subwaveform) and fits it to estimate the range (the distance

80 between the satellite and the sea surface), the SWH and the backscatter coefficient.

81

82 The dataset is freely available at the Open Altimetry Database website of the Technische Universität München

83 (https://openadb.dgfi.tum.de/en/) and includes observations from the following altimetry missions: Envisat (version 3),

84 Jason-1, Jason-1 extended mission, Jason-1 geodetic mission, Jason-2, Jason-2 extended mission, Jason 3, SARAL, SARAL

85 drifting phase, Sentinel 3A and Sentinel 3B. These are provided at a 1 Hz posting rate (equivalent to an along-track

86 resolution of circa 7 km) and cover the period from June 2002 to April 2020, with the exception of one data gap between

87 November 2010 (end of Envisat) and March 2013 (start of SARAL) to the north of 66° N. Data from different missions have

88 been cross-calibrated, so that there are no inter-mission biases.

89

90 Among all the corrections applied to the altimetry data, the geophysical corrections are of particular interest for the purpose

91 of this study. Indeed, to validate the ALES-reprocessed altimetry against the Norwegian tide gauges, the same physical

92 signal must be removed from both datasets. The geophysical corrections applied to the ALES-reprocessed altimetry data

93   include the tidal and the dynamic atmospheric corrections (COSTA user manual,

94   http://epic.awi.de/43972/1/User_Manual_COSTA_v1_0.pdf). The tidal correction is performed using the EOT11a tidal

95   model. The dynamic atmospheric correction (DAC) removes both the wind and the pressure contribution to the sea-level

96   variability at timescales shorter than 20 days, and only the pressure contribution to the sea-level variability at longer

97   timescales. The high-frequency component of the DAC is computed using the Mog2D-G High Resolution barotropic model

98   (Carrère and Lyard, 2003), and it is removed because it would otherwise alias the altimetry data. The low-frequency

99   component accounts for the static response of the sea-level to changes in pressure, a phenomenon also known as inverse

100 barometer effect (IBE), and according to which a 1 hPa increase/decrease in sea-level pressure corresponds to a 1 cm

101 decrease/increase in sea-level. This component is computed by Collecte Localisation Satellites (CLS).

102

103 The producers of ALES flag some of the data as unreliable. More precisely, they recommend excluding observations that fall

104 within a distance of 3 km from the coast and whose sea-level anomaly (SLA), SWH, and standard deviation exceed 2.5 m,

105 11 m, and 0.2 m respectively. We have followed these recommendations with one exception: we have lowered the threshold

106 on the sea-level anomaly from 2.5 to 1.5 m because this choice leads to a better agreement between the tide gauges and the

107 ALES altimetry dataset between Måløy and Rørvik, along the west coast of Norway (Figure 1).

108 **2.2 Tide gauges**

109 The Norwegian Mapping Authority (Kartverket) provides information on observed water levels at 24 permanent tide gauge

110 stations along the coast of Norway. Data are updated, referenced to a common datum, quality checked, and freely distributed

111 through a dedicated web API (api.sehavniva.no).

112

113 Even though most tide gauges provide a few decades of sea-level measurements, in this study we only consider the period

114 between January 2003 and December 2018 because it overlaps with the time-window spanned by the ALES-altimetry

115 dataset. Moreover, we only select 22 of the 24 permanent tide gauges available: we exclude Mausund, since it has no

116 measurements available before November 2010, and Ny-Ålesund, because it is outside of our region of interest.

117

118 Over the period considered, the only tide gauges with missing values are Heimsjø and Hammerfest, with a 1-month gap, and

119 Oslo, with a 2-month gap. We expect the Norwegian set of tide gauges to map the coastal sea-level with a spatial resolution

120 of circa 130 km as it corresponds to the mean distance between adjacent tide gauges. This estimate should be treated only as

121 a first order approximation of the spatial resolution since the distance between adjacent tide gauges varies along the

122 Norwegian coast and ranges from ~30 km, in southern Norway, to ~300 km, in western Norway (more precisely, between

123 Rørvik and Bodø).

124

125
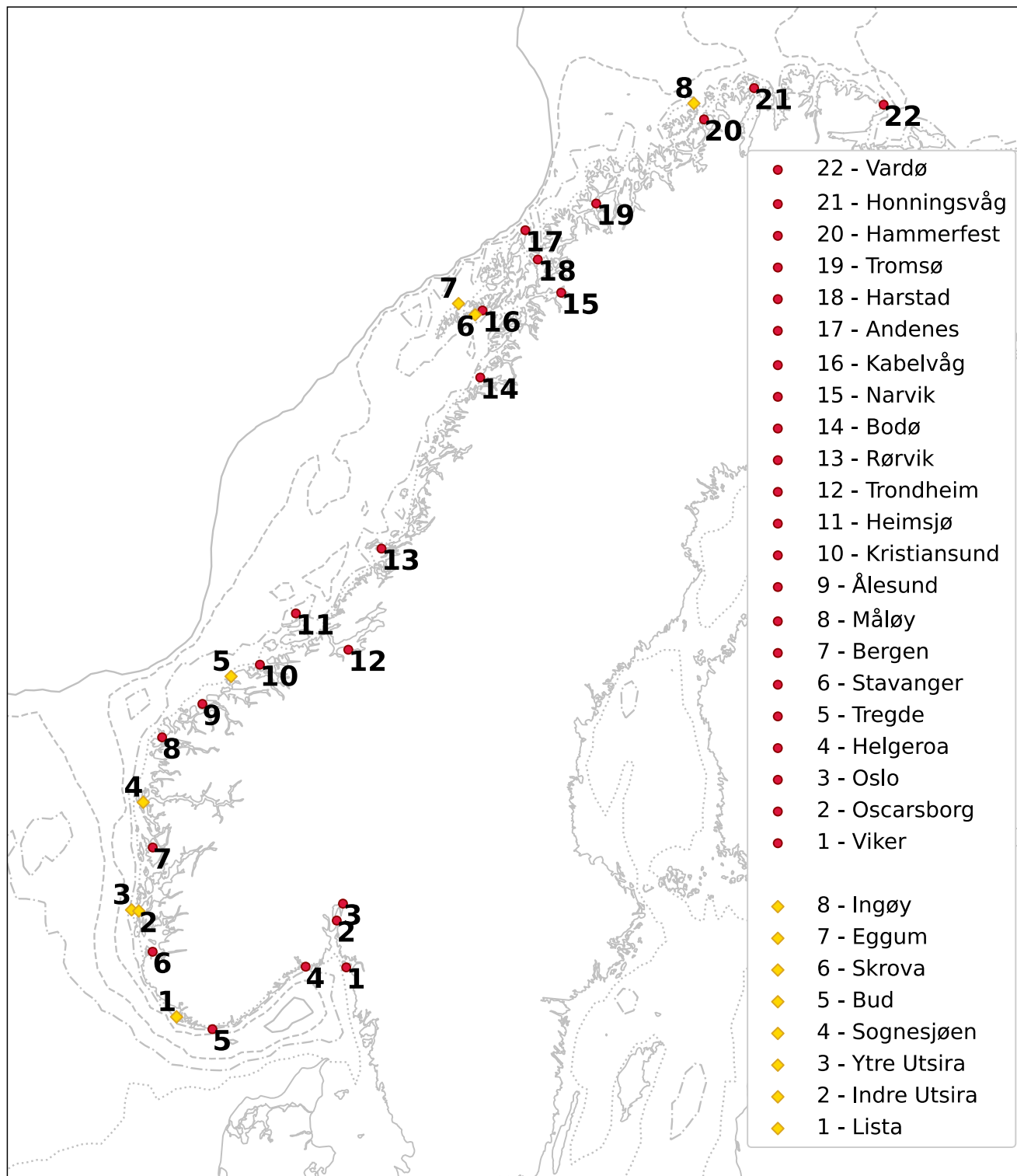
126 **Figure 1: Location of the tide gauges and of the hydrographic stations considered in this study. The solid, dashed, dash-dotted and**
127 **dotted light gray lines indicate the 500 m, 300 m, 150 m, and 50 m isobaths, respectively.**

128

129 A number of geophysical corrections have been applied to the tide gauge data for them to be consistent with the sea-level

130 anomaly from altimetry. These include the effects of the glacial isostatic adjustment (GIA), the nodal tide and the DAC.

131

132 The GIA results from the adjustment of the earth to the melting of the Fennoscandian ice sheet since the last glacial

133 maximum, circa 20 thousand years ago. The earth's relaxation affects substantially the sea-level change relative to the

134 Norwegian coast, with values ranging from approximately 1 up to 5 mm year^{-1} (e.g., Breili et al., 2017). The GIA affects the

135 sea-level because it induces a vertical land movement (VLM) and, to a lesser extent, because it modifies the earth's gravity

136 field. The first effect has been corrected using both GNSS observations and levelling, whereas the second has been corrected

137 using a GIA model (Simpson et al., 2017).

138

139 The low frequency constituents of ocean tide, derived from the EOT11a tidal model, are removed from the tide gauge data as

140 they are from the ALES-reprocessed altimetry dataset. Hammerfest, Honningsvåg and Vardø, the three northernmost tide

141 gauges (Figure 1), are located outside of the EOT11a model domain. Therefore, at these three locations, we remove the low

142 frequency constituents of ocean tide for Tromsø. The constituents in question are the solar semiannual, solar annual, and the

143 nodal tide. For Norway the solar annual astronomical tide is negligible, while the two latter constituents have amplitudes on

144 the order of 1 cm. The nodal tide has a period of approximately 18.61 years and results from the precession of the lunar

145 nodes around the ecliptic (Woodworth, 2012). As our time series are shorter than the nodal cycle, this constituent is not

146 negligible with regards to our trend analysis. None of the solid earth related tides needs to be removed from land-locked tide

147 gauge measurements to produce sea-level records comparable to altimetric sea surface height. Moreover, the ocean pole tide,

148 not provided by the EOF11a, has not been removed from the tide gauge data. However, it is negligible in our region.

149

150 Since we have provided a description of the DAC in the previous section, here we only briefly describe how we have applied

151 it to the tide gauge data. At first, we have monthly averaged the six hourly DAC dataset (available at the AVISO+ website,

152 https://www.aviso.altimetry.fr/en/data/products/auxiliary-products/dynamic-atmospheric-correction.html). Then, for each

153 tide gauge, we have computed the difference between the monthly mean sea-level and DAC at the nearest grid point of the

154 DAC product.

155

2.3 Coastal hydrographic stations

157 Over the time window covered by this study, the Institute of Marine Research (IMR) in Bergen, Norway, has maintained
158 eight permanent hydrographic stations over the Norwegian continental shelf, at a short distance from the coast (Figure
159 1). Data are updated and available at http://www.imr.no/forskning/forskningsdata/stasjoner/index.html.
160

161 Along the Norwegian coast, the number of hydrographic stations is approximately one third the number of tide gauges.
162 Therefore, compared to the tide gauges, the hydrographic stations provide a coarser spatial resolution of the physical
163 properties of the ocean. We find that the distance between adjacent hydrographic stations is approximately 250 km on
164 average. This distance is minimum between the twin stations Indre Utsira/Ytre Utsira and Eggum/Skrova, where it does not
165 exceed 30 km, whereas it is maximum in western Norway, between Bud and Skrova, where it is approximately 670 km.
166

167 As for the tide gauges, we select the temperature and salinity profiles taken between January 2003 and December 2018 for
168 them to overlap with the period covered by the ALES-reprocessed altimetry dataset. The temperature and salinity profiles at
169 each hydrographic station are irregularly sampled and contain missing values (Figure 2). Bud has the largest number of
170 missing values, with 76 gaps out of 192. It is followed by Indre Utsira and Ytre Utsira, with 44 and 41 gaps, respectively.
171 The remaining hydrographic stations have less than 16 gaps each.
172

173 The hydrographic data were used to obtain estimates of the thermosteric and the halosteric sea-level components over the
174 spatial domain considered in this study.
175
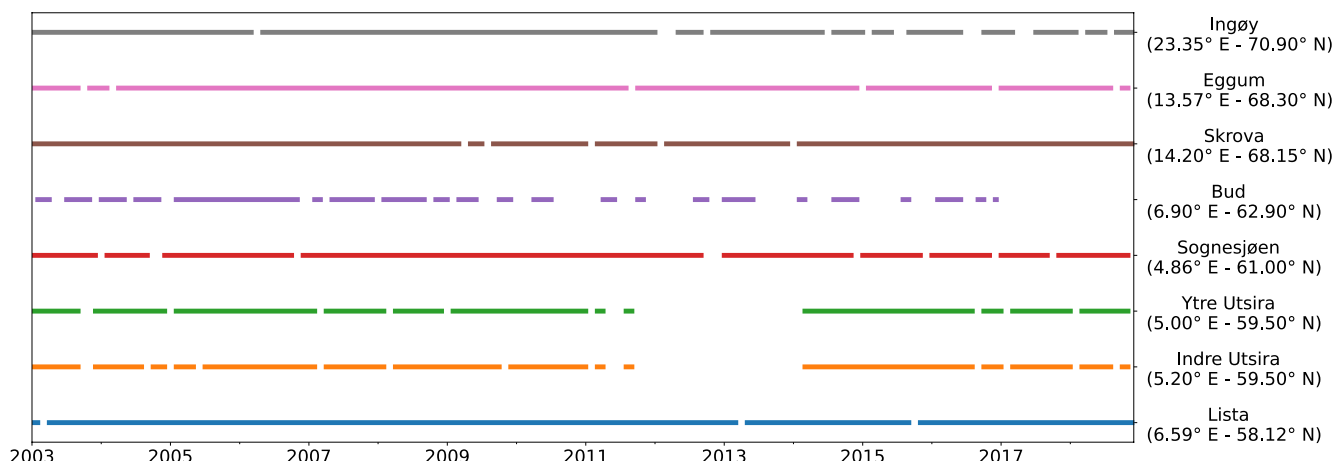
Figure 2: Data available at each hydrographic station between 01 January 2003 and 31 December 2018.

178

2.4 Atmospheric data

180 To quantify the relationship between the thermosteric component of the sea-level at each hydrographic station and surface

181 atmospheric temperature, we use the global monthly mean atmospheric temperature at 2 m from the NCEP/NCAR v2

182 reanalysis dataset (Kalnay et al., 1996) over the period between January 2003 and December 2018. This dataset is provided

183 on a regular grid with a 2.5° x 2.5° spatial resolution.

184

3 Methods

3.1 Sea-level decomposition

187 Following the approach found in previous papers (e.g., Cipollini et al., 2017; Breili et al., 2017), we fit the following

188 function to sea-level records from remote sensing and in situ data:

189

190 $$z(t) = a + b \cdot t + c \cdot \sin(2\pi t + d) + e \cdot \sin(4\pi t + f), \tag{1}$$

191

192 where a is the offset, b the linear trend, c and d the amplitude and the phase of the annual cycle, e and f the amplitude and the

193 phase of the semi-annual cycle. Then, we compare the linear trend, the amplitude and the phase of the annual cycle, and the

194 detrended, deseasoned sea-level signals from remote sensing and in situ data. It is important to note that the use of this

195 formula does not account for interannual variations of the seasonal cycle.

196

3.2 Colocation of satellite altimetry and tide gauges

198 To compare the sea-level from satellite altimetry and tide gauges, we first need to preprocess the altimetry observations since

199 these are not colocated neither in space nor in time with the tide gauges. The colocation consists of two steps. At first, we

200 select the altimetry observations that are located nearby each tide gauge. Then, we average these observations both in space

201 and in time to create, for each tide gauge location, a single time series of monthly mean sea-level anomaly from altimetry.

202

203 During the process, we verify that the selected altimetry observations represent the sea-level variability at each tide gauge

204 location. More precisely, since tide gauges represent the sea-level variability along a stretch of the coast, the distance from

205 the coast and along the coast are adjustable parameters of the selection window. At each station, we test different

206 combinations of the two distances, with the first ranging between 5 and 20 km and the second between 20 and 200 km. Then,

207 we pick the combination that maximizes the linear correlation coefficient between the detrended and deseasoned SLA

208 measured by satellite altimetry and by the tide gauge.

209

210 We choose to maximize the linear correlation coefficient, instead of minimizing the root mean square differences (RMSDs),

211 since the former appears less sensitive in cases when there are few altimetry observations. There is one exception, the Bodø

212 tide gauge, where a very stringent colocation accidentally yields a high correlation. Thus, for Bodø, we select the second

213 highest correlation, which corresponds to a distance from the coast of 20 km and to a distance along the coast of 200 km.

214

215 The results suggest that the spatial pattern associated with the detrended and deseasoned sea-level anomaly extends over

216 hundreds of kilometers. Indeed, the maximum values of the linear correlation coefficients occur for distances along the coast

217 that range between 140 and 200 km, with them being 200 km at 13 out of 22 tide gauges. Moreover, when, for each tide

218 gauge, we manually set the distance from the coast and along the coast, respectively, to 20 km and 200 km, we find that both

219 the linear correlation coefficient and the RMSD vary only little: the first changes by less than 5 %, whereas the second by

220 less than 4.5 %.

221

222 We use the process described above to build a time series of monthly mean sea-level anomaly from altimetry at each tide

223 gauge location. The resulting sea-level time series have no missing values between Viker and Bodø. Instead, to the north of

224 Bodø, they have 29 missing values which result from the lack of altimetry observations between November 2010 and March

225 2013.

226

227 **3.3 Colocation of satellite altimetry and hydrographic stations**

228 We preprocess the altimetry observations to examine the sea-level budget at each hydrographic station since the two datasets

229 are not colocated neither in space nor in time. More precisely, we select all the altimetry observations located within 20 km

230 from the Norwegian coast and within 200 km from each hydrographic station. Then, for each station, we monthly average

231 the altimetry observations to build a sea-level anomaly time series from altimetry. The results in the previous subsection give

232 confidence that the monthly mean sea-level computed over such a large area is representative of the sea-level variability at

233 each hydrographic station.

234

3.4 Monthly mean thermosteric, halosteric and steric sea-level components

To compute the thermosteric and the halosteric components of the sea-level variability at each hydrographic station, we first monthly average the temperature and salinity profiles. Then, at each hydrographic station, we compute the monthly mean thermosteric and the halosteric components of the sea-level as in Richter et al. (2012):

$$\eta_t = \int \alpha(T^*, S^*) \cdot (T - T_0) dz, \qquad (2)$$

$$\eta_s = \int \beta(T^*, S^*) \cdot (S - S_0) dz, \qquad (3)$$

where α and β are the coefficients of thermal expansion and haline contraction, both computed at $T^* = (T + T_0)/2$ and $S^* = (S + S_0)/2$. For each hydrographic station, T_0 and S_0 are reference values and represent time-mean temperature and salinity averaged over the entire water column (Siegismund et al., 2007).

The steric component of the sea-level at each hydrographic station, η_{st}, is simply the sum of the corresponding thermosteric and halosteric components of the sea-level (Gill and Niller, 1973).

4 Comparison of satellite altimetry and tide gauges measurements

In this Section, we assess the quality of the ALES reprocessed coastal altimetry dataset against tide-gauge records by comparing the detrended and deseasoned sea-level variability, the sea-level annual cycle and sea-level trends provided by the remote-sensing and in situ data. We also focus on the stability of linear trend estimates obtained from satellite altimetry (Liebmann et al., 2010; Bonaduce et al., 2016).

4.1 Detrended and deseasoned coastal sea-level
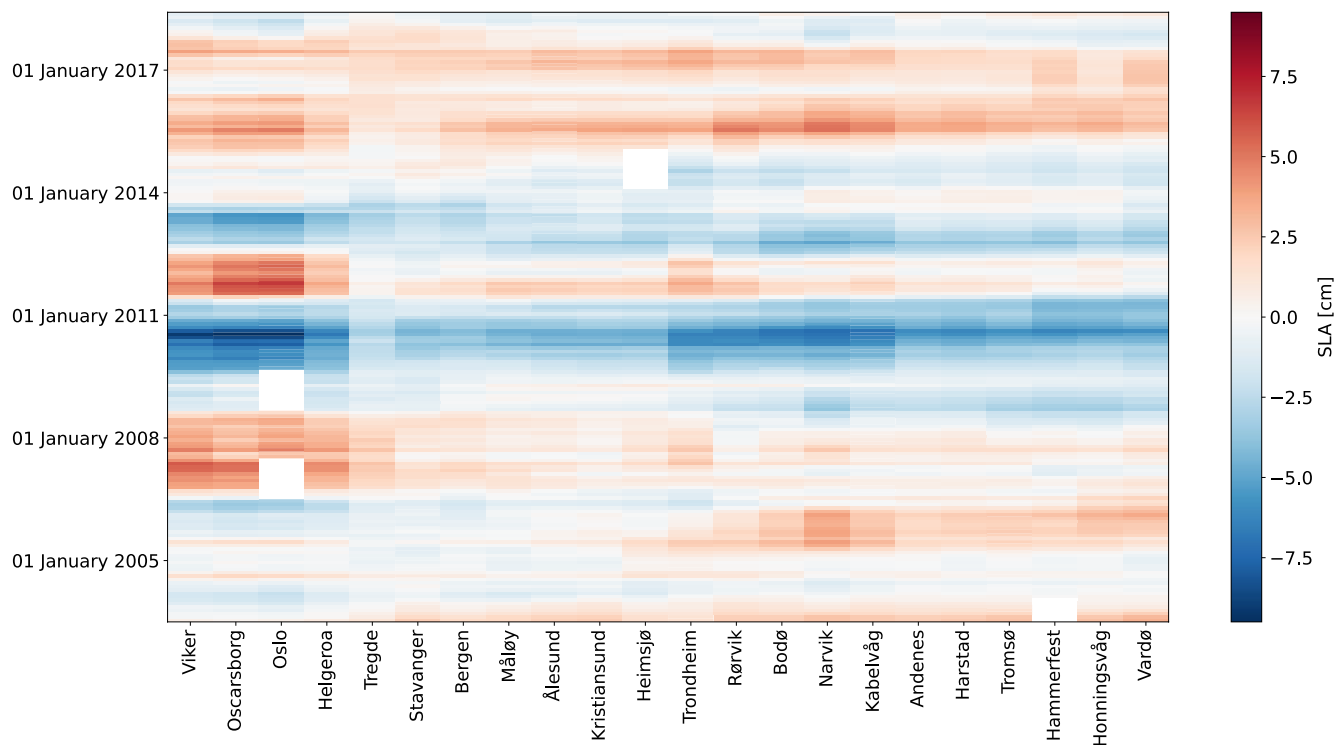
Figure 3: Hovmöller diagram of the detrended and deseasoned monthly mean SLA from tide gauges. The SLA at each tide gauge has been low-pass filtered with a one-year running mean. The tide gauges are displayed on the x-axis. Time is displayed on the y-axis and increases from bottom to top.

Before comparing the detrended and deseasoned SLA from altimetry and tide gauges, we briefly describe how the detrended and deseasoned SLA evolves along the Norwegian coast during the period under study. More precisely, we low-pass filter the detrended and deseasoned SLAs with a one-year running mean to identify their main features at each tide gauge location. Figure 3 shows years when the detrended and deseasoned SLA variations are coherent along the whole Norwegian coast, and years when the sea-level variability occurs at smaller spatial scales (between 100 and 1000 km). As an example, between mid-2009 and the beginning of 2011 circa, the detrended and deseasoned SLA shows negative values of up to -6 cm along the entire Norwegian coast. On the contrary, between 2003 and mid-2009, we note a dipole pattern, with SLA with opposite sign in the south and in the north of Norway. Indeed, up to the beginning of 2006 circa, the Norwegian coast has experienced negative SLA values to the south of Hemsjø and positive SLA to the north of Heimsjø. Over the following three years, the opposite situation has occurred. These results suggest that, although coherent sea-level variability occurs along the Norwegian coast as seen from tide gauges, there are periods when it does not: during these periods, the sea-level variability is likely driven by local changes.

Figure 4: **Comparison between coastal sea-level signals from in situ measurements and area-averaged remote-sensing data. At each tide gauge location, linear correlation coefficient (a) and RMSD (b) between the detrended and deseasoned monthly mean SLA from ALES altimetry dataset and from the tide gauge. The black, dashed line indicates the 66° N parallel.**

Figure 4 shows a very good agreement between the detrended and deseasoned monthly mean SLA from ALES and the tide gauges. The two datasets agree best along the west coast of Norway where, if we exclude Trondheim, the linear correlation coefficients exceed 0.90 and the RMSDs range between 1.5 and 2.5 cm. Satellite altimetry might perform better between Måløy and Rørvik than in southern and northern Norway because of the convergence of altimeter tracks in the region. Trondheim might be an exception because it is located in the Trondheim fjord, where satellite altimetry might not adequately capture local sea-level variations, and where the complex bathymetry and coastline might lead to imprecise geophysical corrections. Similar issues might also occur along the Norwegian Trench, in the Skagerrak and in the Oslo fjord, where the linear correlation coefficients fall between 0.80 and 0.90 and the highest RMSDs range between 2.5 and 4.5 cm. Instead, in northern Norway, where we find linear correlation coefficients between 0.80 and 0.90 (statistically significant at a 0.05 significance level) and RMSDs between 1.5 and 3 cm, the problem might result from the smaller number of altimetry observations in the region. Indeed, only the tracks of Envisat, SARAL, SARAL drifting phase, Sentinel 3A and 3B cover the Norwegian coast north of 66° N.

294

Figure 5: Comparison between coastal sea-level signals from in situ measurements and area-averaged remote-sensing data. At each tide gauge location, standard deviation of the linear correlation coefficients (a) and of the RMSDs (b) computed over each possible combination of the distance from the coast and of the distance from the tide gauge. The black, dashed line indicates the 66° N parallel.

The complex geometry of the Norwegian coast can lead to small-scale variations in sea-level. This can partly explain the difference between the sea-level estimates from tide gauges and from altimetry. Indeed, while the SLA time series measured by the tide gauges are representative for particular locations, those from satellite altimetry, preprocessed as described above, are representative for a spatial domain around the tide-gauge positions. Here, we give an estimate of the geometrical uncertainty on the SLA estimates from satellite altimetry by computing the standard deviation of the linear correlation coefficient and of the RMSD over all the possible combinations of the distance from the coast and of the distance along the coast, as shown in Figure 5.

These results suggests that the detrended and deseasoned SLA in the south vary over smaller spatial scales compared to the north. Indeed, both the linear correlation coefficient and the RMSD in southern Norway depend more on the size of the

311 selection window than in northern Norway. In Figure 5a, we note that the standard deviation of the linear correlation

312 coefficients mainly ranges between 0.15 and 0.20 to the south of Trondheim, whereas it ranges between 0.10 and 0.15 to the

313 north of Trondheim. Likewise, the standard deviation of the RMSD follows a similar spatial pattern, with southern Norway

314 showing higher values compared to northern Norway.

315

4.2 Annual cycle of coastal sea-level

1 - Viker	4 - Helgeroa	7 - Bergen	10 - Kristiansund	13 - Rørvik	16 - Kabelvåg	19 - Tromsø	21 - Honningsvåg
2 - Oscarsborg	5 - Tregde	8 - Måløy	11 - Heimsjø	14 - Bodø	17 - Andenes	20 - Hammerfest	22 - Vardø
3 - Oslo	6 - Stavanger	9 - Ålesund	12 - Trondheim	15 - Narvik	18 - Harstad		
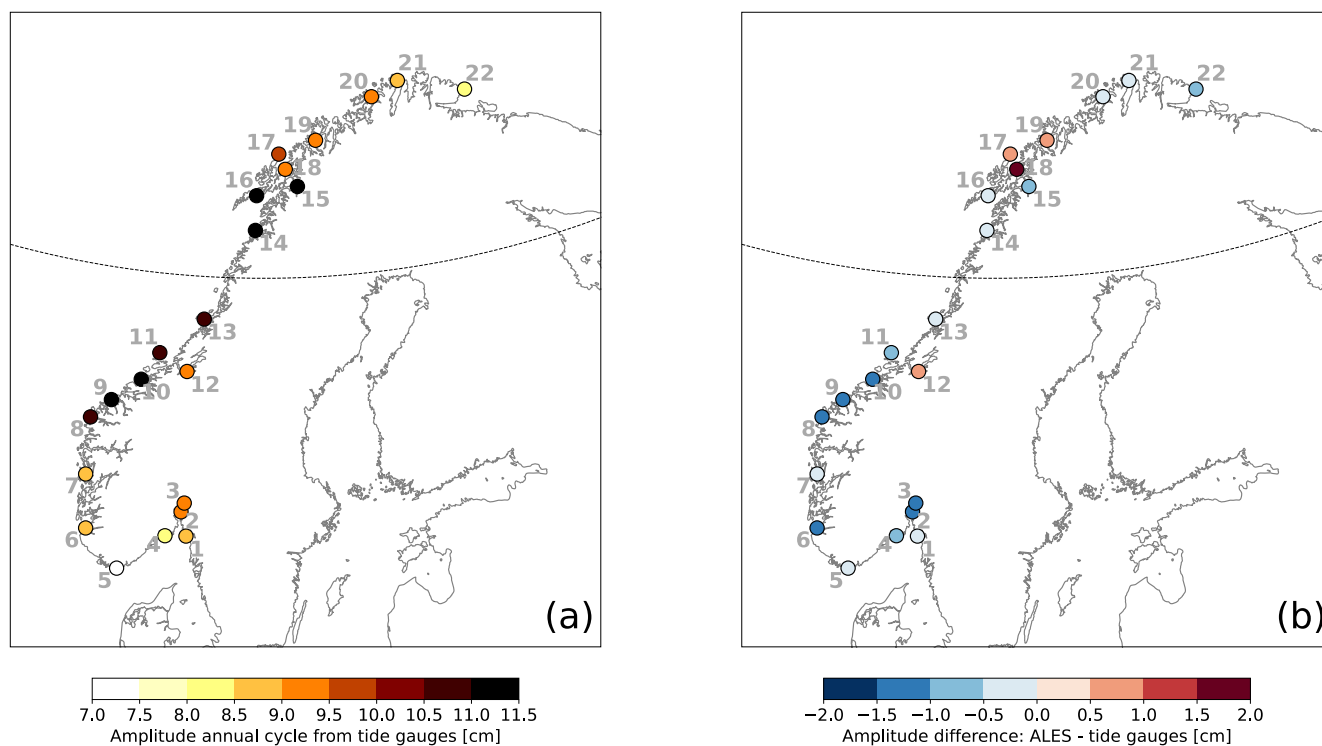
Figure 6: Comparison between the amplitude of coastal sea-level annual cycle from in situ measurements and area-averaged remote-sensing data. At each tide gauge location, amplitude of the annual cycle from the tide gauges (a) and difference between the amplitude of the annual cycle from the ALES-reprocessed altimetry dataset and the tide gauges (b). The black, dashed line indicates the 66° N parallel.

323 Figure 6 andFigure **7** show a good agreement between the annual cycle estimated using the ALES altimetry dataset and the

324 tide gauges. The difference between the amplitudes of the annual cycle from ALES and the tide gauges ranges between -1.2

325 and 1.8 cm. However, at most tide gauge locations (16 out of 22), the differences are much smaller, between -1 and 1 cm,

326 less than 10 % of the amplitude of the corresponding annual cycle (Figure 6a). We note that the differences between the

327 amplitudes are mostly negative along the southern and western coast of Norway and that, to the north of Rørvik, they

328 become smaller, and even change sign at some locations (Figure 6b).

329

330 The difference between the phases of the annual cycle estimated using the ALES altimetry dataset and the tide gauges ranges

331 between -10 and +10 days (Figure 7b). Such a great similarity indicates that both radar altimetry and the tide gauges capture

332 the phase lag of approximately two months between the annual cycle in the north and in the south of Norway. The annual

333 cycle peaks during the second half of September in the Skagerrak and in the Oslo fjord region, in October along the

334 Norwegian Trench and in south-west Norway, and mainly during the first week of November north of Kristiansund.

335

336
337 **Figure 7: Comparison between the phase of coastal sea-level annual cycle from in situ measurements and area-averaged remote-**
338 **sensing data. At each tide gauge location, phase of the annual cycle from the tide gauges (a) and phase difference of the annual**
339 **cycle from the ALES-reprocessed altimetry dataset and from the tide gauges (b). The black, dashed line indicates the 66° N**
340 **parallel.**
341

342

4.2 Linear trend of coastal sea-level
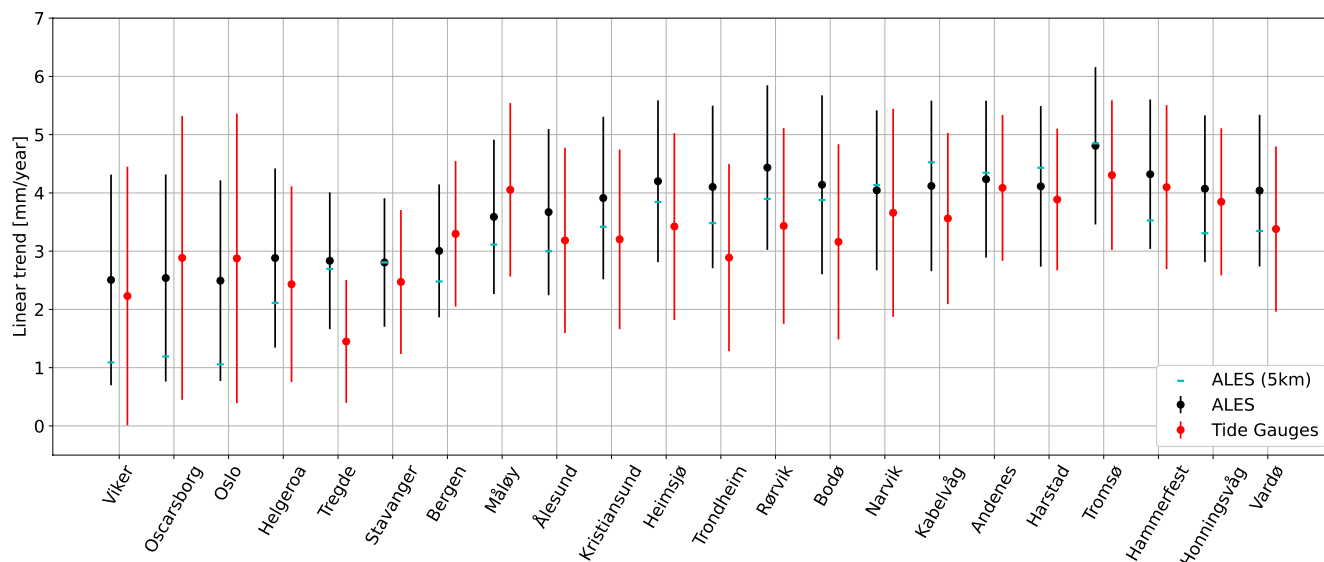
Figure 8: At each tide gauge location, linear trend of the SLA from the ALES-reprocessed altimetry dataset (black dots and cyan dashes) and from tide gauges (red dots). The cyan dashes indicate the linear trend of the sea-level from ALES when we only consider the altimetry observations within 5 km from the coast. The error bars show the 95th confidence intervals of the sea-level trend at each tide gauge location.

The differences between sea-level trend estimate obtained from the in-situ and remote-sensed signals range between -0.8 and 0.8 mm year^{-1} at most tide gauge stations (Figure 8). Both datasets return a similar spatial dependence of the sea-level trend along the Norwegian coast, with the lowest values found in the Skagerrak and the Oslo fjord (between 2 and 3 mm year^{-1}), and the highest to the north of Heimsjø (around 4 mm year^{-1}). Moreover, the two datasets return a similar uncertainty of the sea-level trend at each tide gauge location.

Despite their similarities, we still find that the difference between the sea-level trend from altimetry and tide gauges is statistically significant from zero at a 0.05 significance level at six out of 22 tide gauges. Following Benveniste et al. (2020), we assess the significance in terms of fractal differences (*FDs*). Fractal differences are defined as $FD = |\tau|/(1.97 \cdot SE)$, where $|\tau|$ is the absolute value of the linear trend difference between altimetry and each tide gauge, 1.97 is the critical value of the Student t-test distribution for a 95 % confidence level, and *SE is the standard error*. When $FD > 1$, the difference between the two trends is statistically significant at a 0.05 significance level, a condition that occurs at Tregde, Måløy, Kristiansund, Trondheim, Rørvik and Bodø. Interestingly, only one of these tide gauges is located north of 66° N despite only some of the altimetry missions considered in this study has an inclination exceeding 66° N (namely, Envisat, SARAL,

364   SARAL drifting phase, Sentinel 3A and 3B). Therefore, the fewer altimetry observations to the north of 66° N seem not to

365   deteriorate the agreement between the ALES-reprocessed altimetry and the tide gauges.

366

367   We can partly explain the discrepancy between the sea-level trend obtained from altimetry and the tide gauges by looking at

368   dependency on the distance from the coast. Indeed, from a visual inspection of Figure 8, we note that the sea-level trend

369   from altimetry and the tide gauges show a better agreement along the south-western coast of Norway, between Kristiansund

370   and Rørvik, when we only consider the altimetry observations within 5 km from the coast. This result is backed by the

371   fractal difference technique, which returns values lower than 1 both at Kristiansund, Trondheim, Rørvik and Bodø.

372

373   Following Liebmann et al. (2010), we use the satellite altimetry data to assess how strongly the sea-level trend depends on

374   the time length of the period considered. Each point in Figure 9 shows the sea-level trend computed over the number of the

375   years on the y-axis, up to the year specified on the x-axis. Between 2003 and 2013 circa, we do not find a significant sea-

376   level trend along the Norwegian coast. Indeed, with very few exceptions, the trends are not statistically different from zero at

377   a 0.05 significance level. The exceptions consist in a small number of cases, each characterized by a sea-level trend lower

378   than -4 mm year^{-1}.

379

380   On the contrary, we note a significant positive sea-level trend along the entire coast of Norway when the period considered

381   for the calculation ends in 2015 or later. The linear trends decrease as the length of the period selected increases. When sea-

382   level rates are computed over periods of a few years only, they even exceed 6 mm year^{-1}. Instead, over longer periods of time

383   (e.g. more than 10 years), they mainly range between 3 and 5 mm year^{-1}. A visual inspection of the time series confirms that

384   the sea-level has increased since 2014.
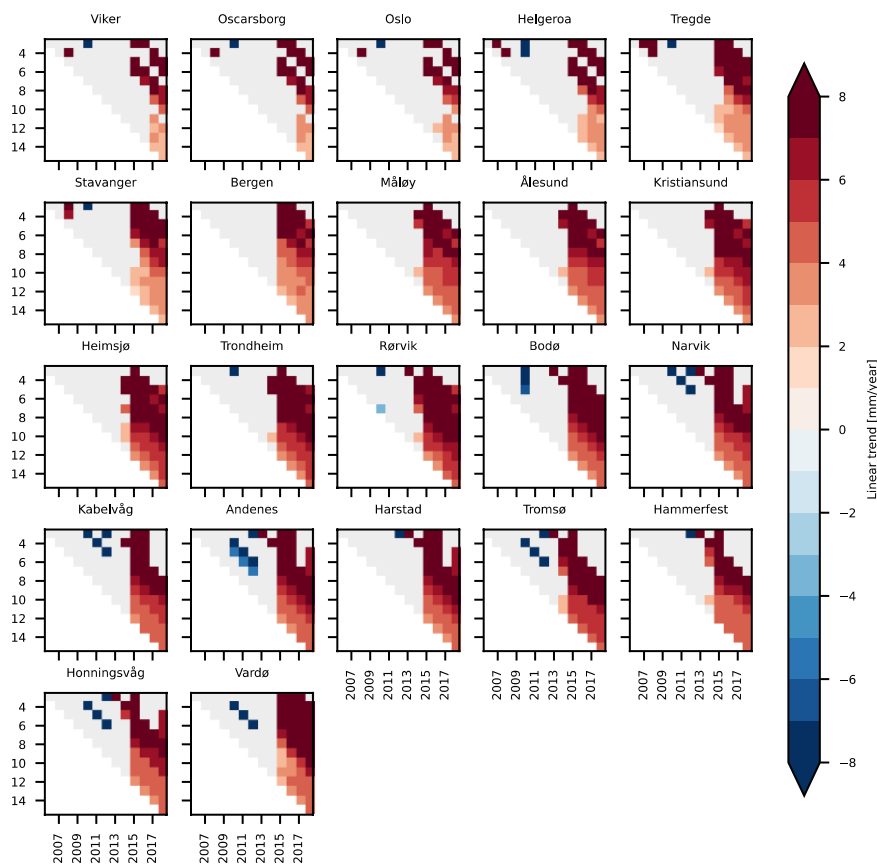
Figure 9: Stability of the sea-level trend along the Norwegian coast. At each tide gauge location, linear trend of the SLA from ALES as a function of the period considered. Each subplot refers to a tide gauge location and shows all the possible trends computed up to the year shown in the x-axis, considering the number of years displayed on the y-axis. For example, the point (x=2014, y=5) in each subplot shows the linear trend of the SLA computed over the 5 years period between 01 January 2009 and 31 December 2014. The light grey colour is used to mask those values that are not significantly different from zero at 0.05 significance level.

5 Sea-level budget

In this Section, we use the Norwegian set of hydrographic stations to assess how temperature and salinity affect the sea-level trend, the sea-level annual cycle and the detrended, deseasoned sea-level variability at different locations along the Norwegian coast.

5.1 Variability of the thermosteric and the halosteric sea-level components

The variability of the thermosteric and the halosteric sea-level components along the Norwegian coast mainly occurs over
two different spatial and temporal scales (Figure 10). Notably, the seasonal cycle dominates the thermosteric sea-level
variability at each hydrographic station and is responsible for the thermosteric sea-level to vary approximately uniformly
along the coast of Norway. On the contrary, the halosteric component shows a variability at shorter spatial- and temporal-
scales, possibly due to the contributions from local rivers. The main exceptions are, due to their proximity, the two sets of
twin hydrographic stations, Indre Utsira-Ytre Utsira and Eggum-Skrova (Figure 1).

Despite these differences, both the thermosteric and the halosteric components of the sea level give a comparable
contribution to the sea-level variability along the Norwegian coast (Figure 10). This ranges approximately between -10 and
10 cm at each hydrographic station.

In the following sections, we investigate the spatial variability of these two components along the Norwegian coast, focusing
on the linear trend, the annual cycle, and the residuals, and on their contribution to the sea-level budget.
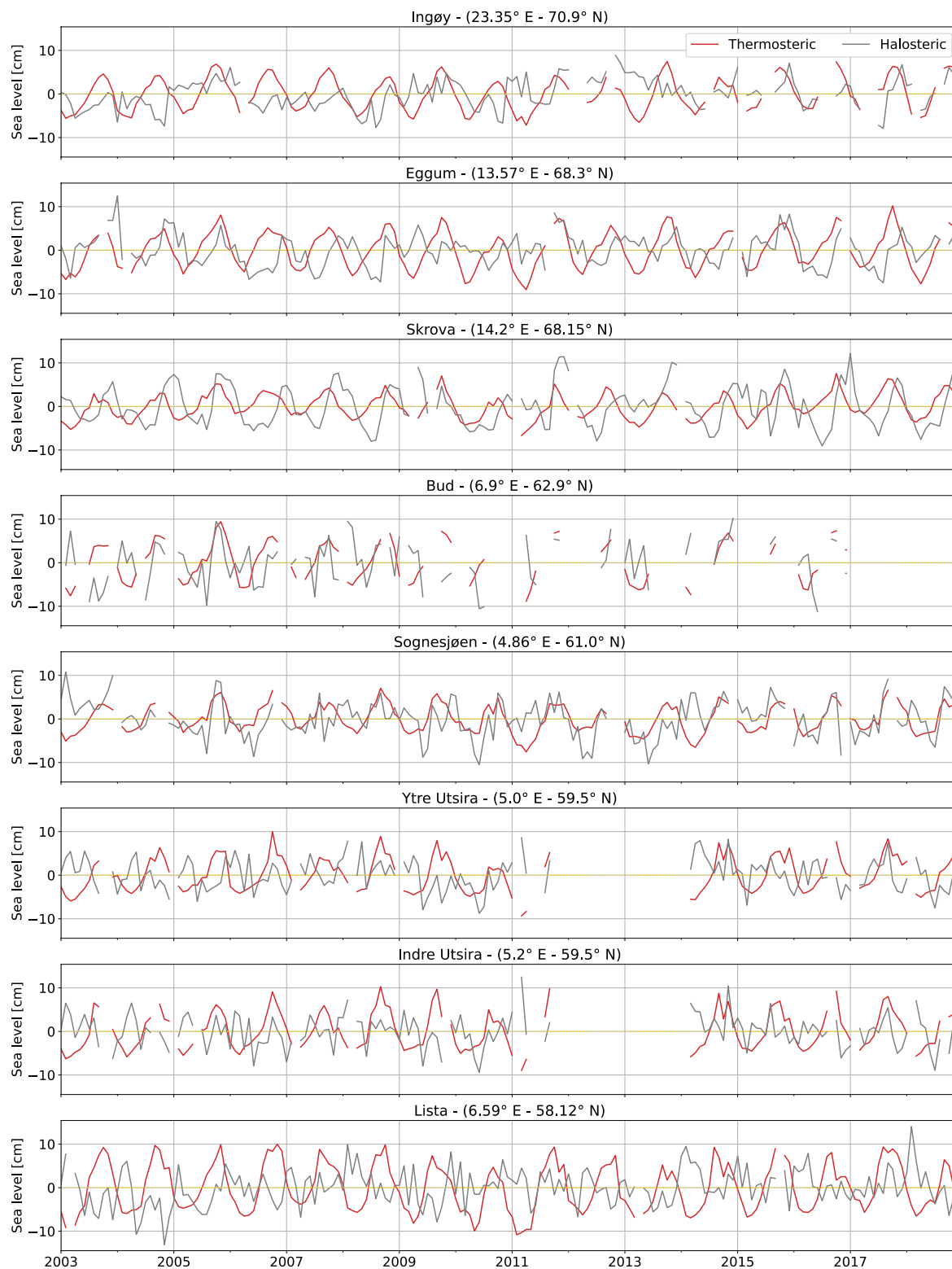
415 **Figure 10: Thermosteric (red) and halosteric (gray) components of the sea-level anomaly at each hydrographic station along the**
416 **Norwegian coast.**

417

418 **5.2 Linear trend of coastal sea-level and its components**

419
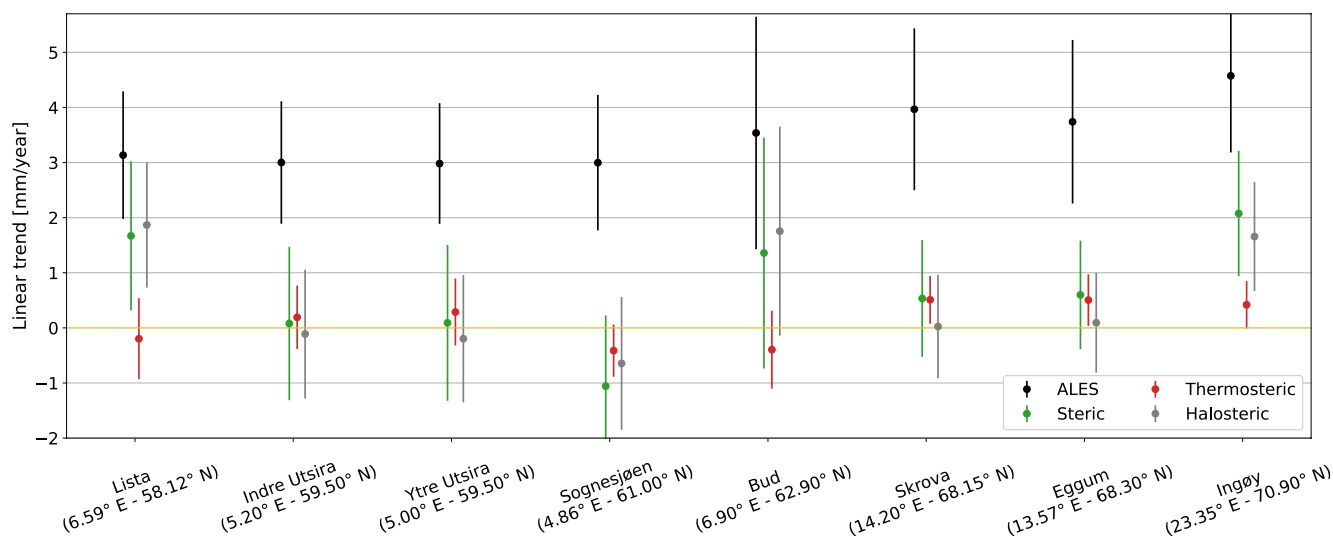
420
421 **Figure 11:** **At each hydrographic station, linear trend of the sea-level from ALES (black dots), and of the steric,**
422 **thermosteric and halosteric components of the sea-level (green, red and grey dots respectively). The bars indicate the**
423 **95 % confidence intervals.**

424

425 In this section, we assess the steric contribution to the sea-level trends along the Norwegian coast, considering monthly

426 averaged coastal altimetry and hydrographic stations. Figure 11 shows the sea-level rates at each hydrographic station

427 considered in this study.

428

429 Over the period 2003-2018, we observe significant steric contributions to coastal sea-level trends, but mostly in the very

430 south and the very north of the Norwegian coast, at Lista and Ingøy, with the steric component explaining between

431 approximately 40–50 % of the sea-level trend estimates obtained from altimetry data. Moreover, when we compare the

432 thermosteric and the halosteric signals at these locations, we note that the latter contributes more than the former to the

433 coastal sea-level trends (up to 60 %).

434

435 At the other locations, the steric contribution to coastal sea-level is either more uncertain or considerably smaller. At Bud,

436 the steric component explains a large fraction of the sea-level trend comparable to the one found at Lista and Ingøy, but,

437 similarly to Lista and Ingøy, this mainly results from salinity changes. However, the uncertainty associated with these

438   estimates are larger at Bud than at the other two stations probably due to the large gaps in the temperature and salinity

439   recordings in the second half of the record. At the remaining five locations, the trends induced by the thermosteric, the

440   halosteric and the steric sea-level are considerably smaller than the altimetry rates. This suggests a larger influence of the

441   non-steric (mass induced) sea-level trend in these areas.

442

443   We note that the results in Figure 11 partly differ from those presented by Richter et al. (2012). Indeed, Richter et al. (2012)

444   shows that the thermosteric sea-level trend exceeds the halosteric sea-level trend at each hydrographic station: while the

445   thermosteric component of the sea-level is positive along the entire Norwegian coast and ranges between approximately 0.5

446   and 1.0 mm year^{-1}, the halosteric component only ranges between -0.3 and 0.3 mm year^{-1}. Between the thermosteric and the

447   halosteric components of the sea-level trends, the latter shows the largest difference with Richter et al. (2012). This is more

448   pronounced at Lista and Ingøy where the sea-level trend difference exceeds 1.5 mm year^{-1}. We can attribute, however, the

449   differences between Richter et al. (2012) and the present work to the different time periods dealt by the two studies: Richter

450   et al. (2012) focused on the 1960–2010 period, whereas here we focus on the shorter 2003–2018 period.

451

452   We can partly explain the temporal and the spatial variations of the linear trend of the thermosteric sea-level anomaly by

453   analysing the air temperature variability at 2 m. Indeed, the thermosteric component and the air temperature at the surface

454   strongly correlate at inter-annual and longer timescales: when we low-pass filter them with a 24-month running mean, the

455   linear correlation coefficient between January 1960 and December 2018 ranges between 0.77 and 0.89 at all the

456   hydrographic stations except for Eggum and Ingøy. A closer look at the thermosteric component of the sea-level at these two

457   locations shows that the drop in correlation might not have a physical origin since it is most likely due to suspiciously high

458   values of the thermosteric component in the 70s and the 80s. Moreover, we find that, in agreement with the results in Richter

459   et al. (2012) and in Figure 11, the linear trend of the atmospheric temperature at 2 m between 1960 and 2010 shows positive

460   values, statistically significant at a 0.05 significance level, at all hydrographic stations, whereas such a condition is satisfied

461   only at Skrova, Eggum and Ingøy between 2003 and 2018. So there was less warming in the past 15 years than during the

462   previous four decades.

463

464   To better understand what causes the spatial difference of the halosteric sea-level trend along the Norwegian coast, we

465   compute the linear trends at each hydrographic station as a function of depth level (Figure 12). The results suggests that the

466   large halosteric sea-level trends at Lista, Bud and Ingøy occur for different reasons. At Lista, the high values result from a

467   freshening in the bottom layer of the water column, below 100 m depth. At Bud, they mainly result from a freshening of the

468   upper layer of the water column, between 20 and 50 m. Instead, at Ingøy, they are mainly caused by a freshening of the

469   entire water column, with it being particularly intense between 50 and 150 m depth, suggesting remote effects rather than the

470   contribution from local rivers.

471
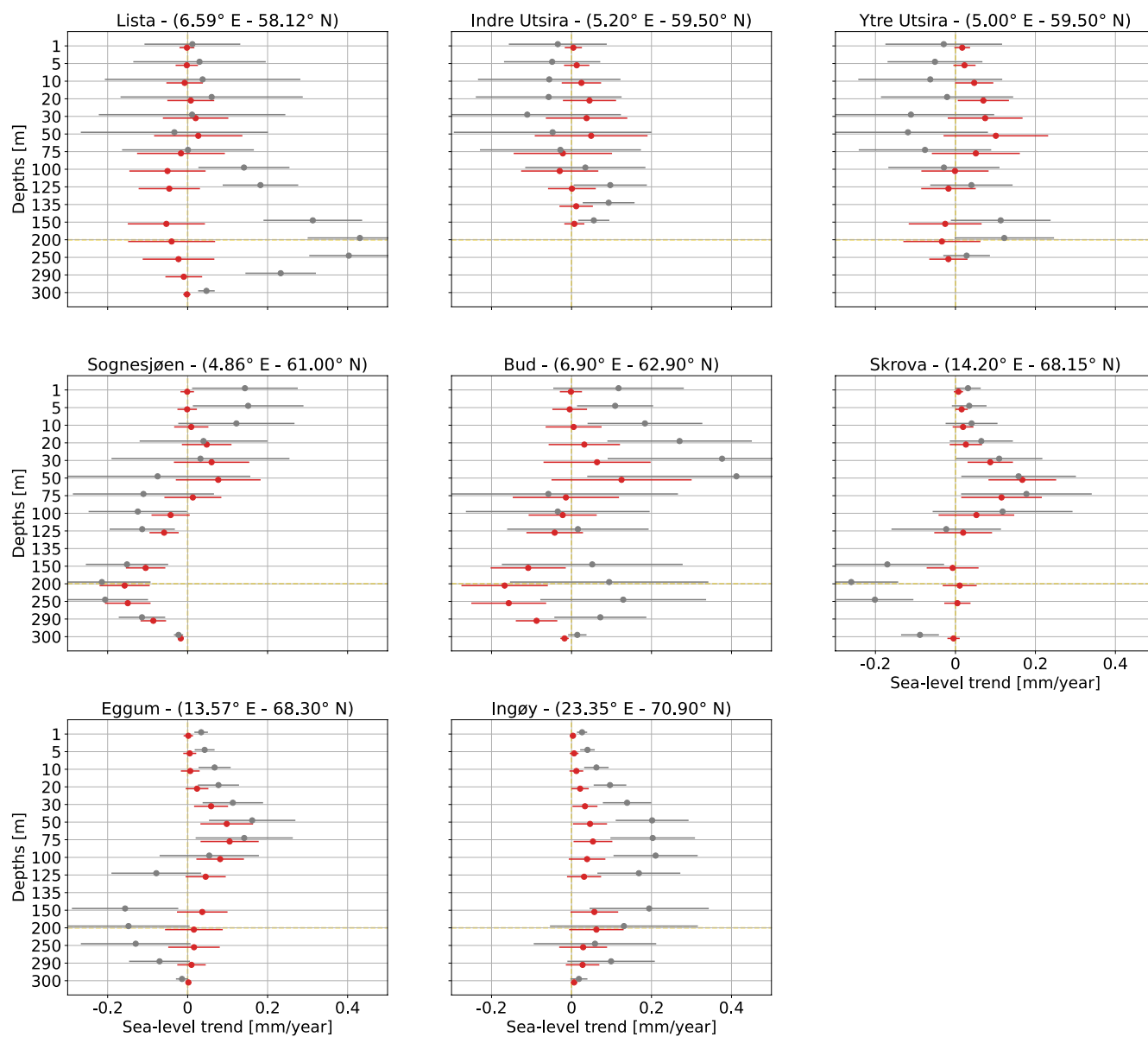
472
473 **Figure 12: Linear trend of the thermosteric (red dots) and the halosteric (grey dots) at each depth level of each hydrographic**
474 **station. The bars indicate the 95 % confidence interval.**
475

476

5.2 Annual cycle of coastal sea-level and its components

477

478 We now assess the thermosteric, halosteric, and steric components of the sea-level annual cycle at each hydrographic station

479 along the Norwegian coast.

480

481 Contrary to what we observe for the sea-level trends, the steric sea-level gives a non-negligible contribution to the sea-level

482 annual cycle along the entire Norwegian coast (Table 1). Indeed, the steric signal explains more than 60 % of the sea-level

483 annual cycle at six out of eight hydrographic stations.

484

485 In Table 1, we note that the annual cycle of steric sea-level is largely associated with ocean thermal expansion: except for

486 Skrova, the thermosteric component shows larger amplitudes than the halosteric component along the Norwegian coast. The

487 largest differences are observed at Lista, Indre Utsira and Ytre Utsira where the thermosteric component exceeds the

488 halosteric sea-level signal by 3.2, 5.4 and 4.2 times, respectively.

489

490 While the phase of the thermosteric component changes by less than half a month along the entire Norwegian coast, the

491 halosteric component shows a higher variability. In southern Norway, up to Ytre Utsita, the thermosteric and the halosteric

492 sea-level components have almost opposite phase: the thermosteric sea-level peaks in the second half of October, whereas

493 the halosteric component peaks at the beginning of the year (Table 2). To the north of Ytre Utsira, the lag between the

494 thermosteric and the halosteric components of the sea-level decreases since the halosteric annual cycle peaks between

495 October and November at Sognesjøen, and in December from Bud to Ingøy.

496

497 **Table 1: At each hydrographic station, amplitude of the annual cycle of the thermosteric, halosteric and steric**
498 **components of the monthly mean sea-level, and amplitude of the annual cycle of the sea-level measured from**
499 **altimetry. The uncertainty indicates the 95 % confidence interval. Units are cm.**

	Thermosteric	Halosteric	Steric	Total sea-level
Lista (6.59° E - 58.12° N)	6.9 ± 0.5	2.2 ± 0.7	5.5 ± 0.9	7.1 ± 0.7
Indre Utsira (5.20° E - 59.50° N)	5.6 ± 0.4	1.0 ± 0.8	4.6 ± 1.0	7.6 ± 0.8
Ytre Utsira (5.00° E - 59.50° N)	4.8 ± 0.4	1.2 ± 0.8	3.7 ± 1.0	7.6 ± 0.8

Sognesjøen (4.86° E - 61.00° N)	3.9 ± 0.3	2.4 ± 0.8	6.2 ± 0.8	8.6 ± 0.8
Bud (6.90° E - 62.90° N)	5.8 ± 0.4	2.9 ± 1.2	7.0 ± 1.1	9.6 ± 1.2
Skrova (14.20° E - 68.15° N)	3.4 ± 0.3	4.5 ± 0.6	6.2 ± 0.7	11.1 ± 1.0
Eggum (13.57° E - 68.30° N)	5.4 ± 0.3	2.7 ± 0.6	6.7 ± 0.6	10.9 ± 1.0
Ingøy (23.35° E - 70.90° N)	4.9 ± 0.3	1.7 ± 0.6	5.5 ± 0.7	9.0 ± 0.9

500

501 **Table 2: At each hydrographic station, phase of the annual cycle of the thermosteric, halosteric and steric**
502 **components of the monthly mean sea-level, and phase of the annual cycle of the sea-level measured from altimetry.**
503 **The uncertainty indicates the 95 % confidence interval. Units are months: 0 stands for 01 January, whereas 12 for 31**
504 **December.**

	Thermosteric	Halosteric	Steric	Total sea-level
Lista (6.59°E - 58.12°N)	8.7 ± 0.1	1.3 ± 0.7	9.2 ± 0.3	9.4 ± 0.2
Indre Utsira (5.20°E - 59.50°N)	8.5 ± 0.1	1.8 ± 1.5	8.6 ± 0.4	9.6 ± 0.2
Ytre Utsira (5.00°E - 59.50°N)	8.9 ± 0.2	2.6 ± 1.3	9.0 ± 0.5	9.6 ± 0.2
Sognesjøen (4.86°E - 61.00°N)	8.9 ± 0.1	9.8 ± 0.6	9.2 ± 0.3	9.6 ± 0.2
Bud (6.90°E - 62.90°N)	8.9 ± 0.1	11.5 ± 0.7	9.7 ± 0.3	9.9 ± 0.2

Skrova (14.20°E - 68.15°N)	8.6 ± 0.2	11.2 ± 0.3	10.1 ± 0.2	10.2 ± 0.2
Eggum (13.57°E - 68.30°N)	8.8 ± 0.1	11.3 ± 0.4	9.6 ± 0.2	10.2 ± 0.2
Ingøy (23.35°E - 70.90°N)	8.9 ± 0.1	11.4 ± 0.7	9.3 ± 0.3	10.1 ± 0.2

505
506

507 **5.3 Detrended and deseasoned coastal sea-level and its components**
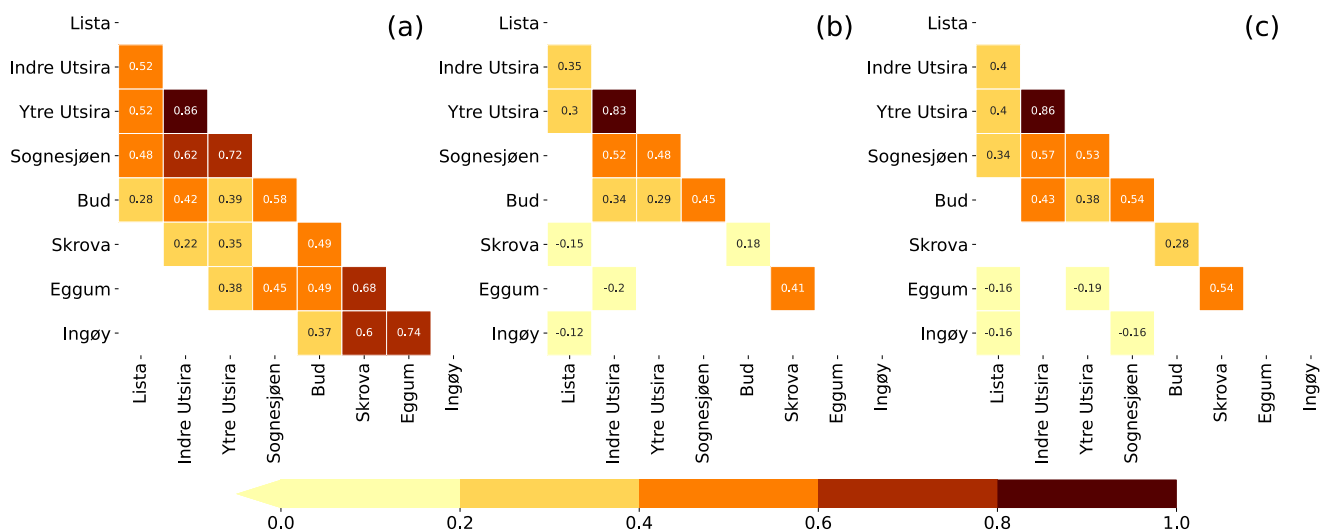
508
509 **Figure 13: Correlation matrices of the detrended and deseasoned thermosteric (a), halosteric (b) and steric (c) components of the**
510 **sea-level at each hydrographic station. Correlation values that are not significant at a 0.05 significance level have been omitted.**
511

512 The detrended and deseasoned thermosteric sea-level along the Norwegian coast shows a larger spatial variability compared

513 to the detrended, deseasoned halosteric component (Figure 13). The correlation matrix of the thermosteric sea-level (Figure

514 13a) shows larger values compared to the one obtained considering halosteric sea-level signals (Figure 13b). As an example,

515 while the minimum linear correlation coefficient between two adjacent hydrographic stations in Figure 13a is 0.49, it is only

516 0.18 in Figure 13b. We briefly discuss the small spatial scale variability of the halosteric sea-level component along the

517 Norwegian coast in the Discussion and conclusions section of the paper.

518

519 From Figure 13c, we also note that the values of the correlation matrix of the steric sea-level fall in between those of the

520 thermosteric and of the halosteric components. This suggests that the thermosteric and halosteric components of the sea-level

521 give a similar contribution to the sea-level variability along the Norwegian coast.

522

523 **6 Discussion and conclusions**

524 In this paper, we have first assessed the ability of the ALES-reprocessed altimetry dataset to capture the Norwegian sea-level

525 variability over a range of timescales. Then, we have used data from hydrographic stations to quantify the steric

526 contributions and partition the sea-level variability along the coast of Norway.

527

528 When compared to conventional altimetry (Breili et al., 2017), the ALES-reprocessed altimetry dataset provides estimates of

529 the sea-level trend along the coast of Norway that better agree with those from tide gauges. Unfortunately, we cannot

530 directly compare the linear trends in this work with those in Breili et al. (2017) since they focus on a different period and, the

531 sea-level trend along the Norwegian coast strongly depends on the length of the time-window considered (Figure 9). When

532 comparing those altimetry datasets with tide-gauge records in terms of linear trend computed over a common time-window,

533 ALES shows an improvement over the conventional open ocean retracker. This is particularly evident in northern Norway,

534 between Bodø and Tromsø, where the difference between the linear trend from ALES and the tide gauges are small (up to

535 0.7 mm year^{-1}), compared to circa 1 to 3 mm year^{-1} obtained using a conventional altimetry dataset.

536

537 The results obtained from the ALES dataset also suggest that along the north-western coast of Norway, between Ålesund and

538 Bodø, the accuracy of remote-sensed sea-level records might depend on the distance from the coast. Indeed, the agreement

539 between the sea-level trends estimated from satellite altimetry and the tide gauges increases as we restrict the altimetry

540 observations to 5 km from the coast. Previous studies (e.g., Cazenave et al., 2018; Marti et al., 2019; Gouzenes et al., 2020)

541 have also reported changes in the sea-level trend within a few kilometres in several regions of the globe and they have

542 argued for their physical origin. The contribution of winds, river runoff and ~~wave forcing~~ are reported to explain the

543 departure of the sea-level trend along the coast from that in the open ocean. However, while previous studies have mostly

544 observed a sea-level trend increase towards the coast, our results suggest the opposite. Unfortunately, in this study, we

545 cannot use the in situ data to understand this feature. Indeed, Bud is the only hydrographic station in the region and, due to

546 its numerous gaps, it does not allow for a clear quantification of the thermosteric and halosteric contributions to the sea-level

547 trend. A dedicated study that uses both a 20 Hz coastal altimetry dataset and a high resolution ocean reanalysis, such as

548 NorShelf (Röhrs et al., 2018), could help better understand whether the sea-level trend actually decreases towards the coast

549 and why.

550

551 Even though the ALES altimetry dataset tend to underestimate and overestimates the amplitude of the annual cycle,

552 respectively, to the south and to the north of Kabelvåg, a comparison with Volkov and Pujol (2012) shows that it better

553 captures the sea-level annual cycle along the coast of Norway with respect to the gridded sea-level altimetry products. In that

554 study, the authors have considered six tide gauges along the Norwegian coast, namely, Kristiansund, Rørvik, Andenes,

555 Hammerfest, Honningsvåg and Vardø to assess the quality of satellite altimetry maps at the northern high latitudes. Except

556 for Andenes, we note that the ALES-reprocessed coastal altimetry dataset allows for more accurate estimates of the sea-level

557 annual cycle, reducing the differences with the in situ sea-level records by a factor of 3 to 6 compared to gridded satellite

558 altimetry products.

559

560 A sea-level budget analysis, performed at each hydrographic station, shows that the halosteric component of sea-level

561 variability strongly influences the spatial variability of the sea-level annual cycle along the Norwegian coast. Indeed, while

562 the thermosteric component peaks in October along the entire coast of Norway, the halosteric component peaks at the

563 beginning of the year in southern Norway, between October and November at Sognesjøen, and in December from the middle

564 to the north of Norway. When we compute the same analysis, but considering halosteric sea-level signals over different

565 depth ranges (Figure 14), we note that the spatial variability of the halosteric component of the sea-level results from surface

566 processes: while the annual cycle of the halosteric signal at the surface has a maximum in June in southern Norway, it peaks

567 later in the year as one moves northward. The result for southern Norway agrees with Janssen et al. (1999) and Hordoir et al.

568 (2013) who show that surface salinity has a minimum in June because of the combined effect of river runoff and the

569 freshwater flux from the Baltic Sea. Instead, the result for northern Norway might follow from the advection of the

570 freshwater from the Baltic which needs a few months to reach northern Norway (Koszalka et al., 2013).

571
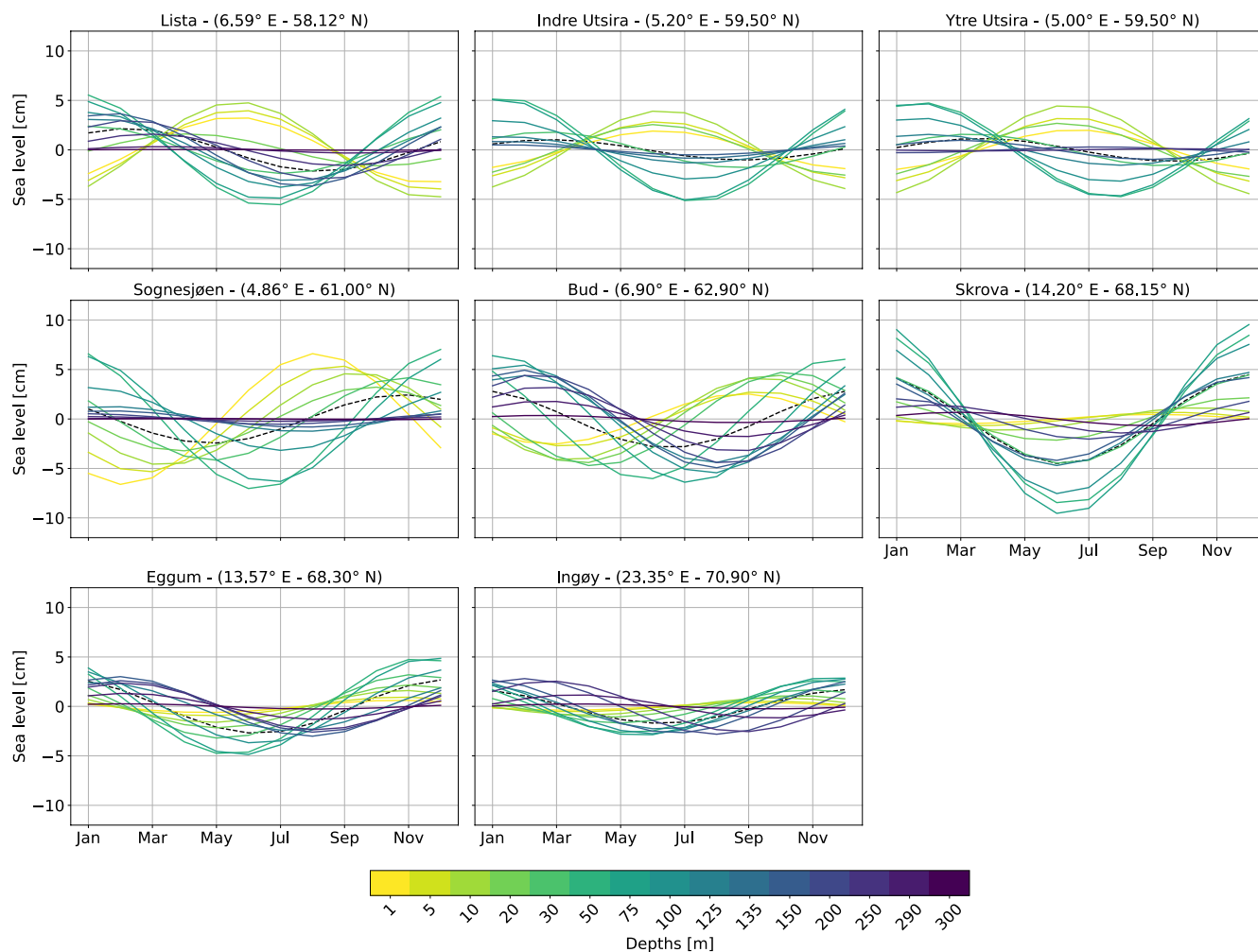
Figure 14: At each hydrographic station, annual cycle of the halosteric component of the sea-level at each depth level. We assign to each colour of the viridis colorbar a depth level, with the colours getting darker with depth. The black, dashed line shows the annual cycle of the halosteric component computed over the entire water column at each hydrographic station location.

The detrended and deseasoned sea-level varibility along the Norwegian shelf resembles the along-slope wind index proposed by Chafik et al. (2019). We note that the similarities between the two are stronger along the western and the northern coast of Norway than in the south. Indeed, from Olso to Ålesund, those SLA signals depart from the along-slope winds index between 2003 and 2008, probably due to local effects, such as the Baltic outflow. We refer to local effects since Chafik et al. (2019) attributed the interannual sea level variability over the northern European continental shelf to the along-slope winds, which might regulate the exchange of water between the open ocean and the shelf through Ekman transport.

The small-scale variability of the detrended and deseasoned sea-level halosteric component (Figure 13) does not reconcile with the good agreement between tide gauge sea-level signals and the ALES-reprocessed altimetry dataset. Indeed, to

586 compare the two datasets, we have averaged the satellite altimetry observations over an area a few hundreds of kilometres

587 wide around each tide gauge. However, Figure 13 suggests that the estimates of the halosteric component can change

588 significantly over an area of this size. Furthermore, while this component has a magnitude comparable to that of the

589 detrended, deseasoned SLA (not shown), it only explains a small fraction (from 3 to 11 %) of the difference between the sea-

590 level signals from altimetry and the tide gauges.

591

592 Future work is thus warranted to understand whether the small-scale variability of the halosteric component of the sea-level

593 along the Norwegian coast results from measurement issues. For example, ocean salinity is measured approximately once a

594 week at Skrova and approximately twice a month at the remaining hydrographic stations: this aliases the sub-weekly salinity

595 variations into the lower frequency components and, consequently, might significantly alter the monthly mean salinity

596 values. A new study, which takes benefit from ships of opportunity, synergies between different observational platforms and

597 ocean models, could help clarify this issue.

598

599 To conclude, we have demonstrated the advantage of the ALES-retracker over the conventional open ocean retracker along

600 the coast of Norway. The retracking of earlier altimeter missions would, however, be necessary to provide a more accurate

601 estimate of the sea level variability along the coast of Norway and possibly used to understand whether the sea-level in the

602 region is accelerating. Still, this paper gives confidence that the ALES-reprocessed altimetry dataset can be fruitfully used to

603 measure coastal sea level variations in regions poorly covered by tide gauges.

604

605 **Data availability**

606 The tide gaude data are available and distributed through a dedicated web API (api.sehavniva.no). The ALES-reprocessed

607 satellite altimetry dataset is available at the Open Altimetry Database website of the Technische Universität München

608 (https://openadb.dgfi.tum.de/en/). The hydrographic stations dataset are updated and available at

609 http://www.imr.no/forskning/forskningsdata/stasjoner/index.html. The NCEP/NCAR v2 dataset is available at

610 https://psl.noaa.gov/data/gridded/data.ncep.reanalysis2.html.

611

612 **Author contribution**

613 FM, AB, LC and LB designed the research study. JEØN removed the geophysical signal from the sea-level measured by the

614 tide gauges. FM wrote the code to analyse the data. All authors contributed to the analysis of the results, and to the writing

615 and the editing of the paper.

616

617 **Competing interests**

618 The authors declare that they have no conflict of interest.

619

Acknowledgements

All products are computed based on altimetry missions operated by NASA/CNES (TOPEX, Jason-1), ESA (ERS-1/2,

Envisat, Cryosat-2), USNavy/NOAA (GFO), CNES/NASA/Eumetsat/NOAA (Jason-2, Jason-3), ISRO/CNES (SARAL),

and EUMETSAT (Sentinel-3). The original data sets are disseminated by AVISO, ESA, NOAA, and PODAAC. Michael

Hart-Davis (TUM) is kindly acknowledged for providing the EOT11a tidal model data.

625
626

627

References

Benveniste, J., Birol, F., Calafat, F., Cazenave, A., Dieng, H., Gouzenes, Y., Legeais, J. F., Léger, F., Niño, F., Passaro, M.,

Schwatke, C., and Shaw, A.: Coastal sea level anomalies and associated trends from Jason satellite altimetry over 2002-

2018, 7, 1–17, https://doi.org/10.1038/s41597-020-00694-w, 2020.

Bonaduce, A., Pinardi, N., Oddo, P., Spada, G., and Larnicol, G.: Sea-level variability in the Mediterranean Sea from

altimetry and tide gauges, 47, https://doi.org/10.1007/s00382-016-3001-2, 2016.

Breili, K., Simpson, M. J. R., and Nilsen, J. E. Ø.: Observed sea-level changes along the Norwegian coast, 5,

https://doi.org/10.3390/jmse5030029, 2017.

Carrère, L. and Lyard, F.: Modeling the barotropic response of the global ocean to atmospheric wind and pressure forcing -

Comparisons with observations, 30, https://doi.org/10.1029/2002GL016473, 2003.

Cazenave, A., Palanisamy, H., and Ablain, M.: Contemporary sea level changes from satellite altimetry: What have we

learned? What are the new challenges?, 62, https://doi.org/10.1016/j.asr.2018.07.017, 2018.

Chafik, L., Nilsson, J., Skagseth, and Lundberg, P.: On the flow of Atlantic water and temperature anomalies in the Nordic

Seas toward the Arctic Ocean, 120, https://doi.org/10.1002/2015JC011012, 2015.

Chafik, L., Nilsen, J. E. Ø., Dangendorf, S., Reverdin, G., and Frederikse, T.: North Atlantic Ocean Circulation and Decadal

Sea Level Change During the Altimetry Era, 9, https://doi.org/10.1038/s41598-018-37603-6, 2019.

Cipollini, P., Benveniste, J., Birol, F., Joana Fernandes, M., Obligis, E., Passaro, M., Ted Strub, P., Valladeau, G.,

Vignudelli, S., and Wilkin, J.: Satellite altimetry in coastal regions, in: Satellite Altimetry Over Oceans and Land Surfaces,

https://doi.org/10.1201/9781315151779, 2017.

647 Eyring, V., Bony, S., Meehl, G. A., Senior, C. A., Stevens, B., Stouffer, R. J., and Taylor, K. E.: Overview of the Coupled
648 Model Intercomparison Project Phase 6 (CMIP6) experimental design and organization, 9, https://doi.org/10.5194/gmd-9-
649 1937-2016, 2016.

650 Gill, A. E. and Niller, P. P.: The theory of the seasonal variability in the ocean, 20, https://doi.org/10.1016/0011-
651 7471(73)90049-1, 1973.

652 Gouzenes, Y., Léger, F., Cazenave, A., Birol, F., Bonnefond, P., Passaro, M., Nino, F., Almar, R., Laurain, O., Schwatke, C.,
653 Legeais, J.-F., and Benveniste, J.: Coastal Sea Level rise at Senetosa (Corsica) during the Jason altimetry missions,
654 https://doi.org/10.5194/os-2020-3, 2020.

655 Hordoir, R., Dieterich, C., Basu, C., Dietze, H., and Meier, H. E. M.: Freshwater outflow of the Baltic Sea and transport in
656 the Norwegian current: A statistical correlation analysis based on a numerical experiment, 64,
657 https://doi.org/10.1016/j.csr.2013.05.006, 2013.

658 Janssen, F., Schrum, C., and Backhaus, J. O.: A climatological data set of temperature and salinity for the Baltic Sea and the
659 North Sea, 51, https://doi.org/10.1007/BF02933676, 1999.

660 Ji, M., Reynolds, R. W., and Behringer, D. W.: Use of TOPEX/Poseidon sea level data for Ocean analyses and ENSO
661 prediction: Some early results, 13, https://doi.org/10.1175/1520-0442(2000)013<0216:UOTPSL>2.0.CO;2, 2000.

662 Kalnay, E., Kanamitsu, M., Kistler, R., Collins, W., Deaven, D., Gandin, L., Iredell, M., Saha, S., White, G., Woollen, J.,
663 Zhu, Y., Chelliah, M., Ebisuzaki, W., Higgins, W., Janowiak, J., Mo, K. C., Ropelewski, C., Wang, J., Leetmaa, A.,
664 Reynolds, R., Jenne, R., and Joseph, D.: The NCEP/NCAR 40-year reanalysis project, 77, https://doi.org/10.1175/1520-
665 0477(1996)077<0437:TNYRP>2.0.CO;2, 1996.

666 Koszalka, I., LaCasce, J. H., and Mauritzen, C.: In pursuit of anomalies-Analyzing the poleward transport of Atlantic Water
667 with surface drifters, 85, https://doi.org/10.1016/j.dsr2.2012.07.035, 2013.

668 Lichter, M., Vafeidis, A. T., Nicholls, R. J., and Kaiser, G.: Exploring data-related uncertainties in analyses of land area and
669 population in the "Low-Elevation Coastal Zone" (LECZ), 27, https://doi.org/10.2112/JCOASTRES-D-10-00072.1, 2011.

670 Liebmann, B., Dole, R. M., Jones, C., Bladé, I., and Allured, D.: Influence of choice of time period on global surface
671 temperature trend estimates, 91, https://doi.org/10.1175/2010BAMS3030.1, 2010.

672 Madsen, K. S., Høyer, J. L., Suursaar, Ü., She, J., and Knudsen, P.: Sea Level Trends and Variability of the Baltic Sea From
673 2D Statistical Reconstruction and Altimetry, 7, https://doi.org/10.3389/feart.2019.00243, 2019.

674 Marti, F., Cazenave, A., Birol, F., Passaro, M., Léger, F., Niño, F., Almar, R., Benveniste, J., and Legeais, J. F.: Altimetry-
675 based sea level trends along the coasts of Western Africa, https://doi.org/10.1016/j.asr.2019.05.033, 2019.

676 Nerem, R. S., Chambers, D. P., Choe, C., and Mitchum, G. T.: Estimating Mean Sea Level Change from the TOPEX and
677 Jason Altimeter Missions, 33, https://doi.org/10.1080/01490419.2010.491031, 2010.

678 Oppenheimer, M., Glavovic, B., Hinkel, J., van de Wal, R., Magnan, A. K., Abd-Elgawad, A., Cai, R., Cifuentes-Jara, M.,
679 DeConto, R. M., Ghosh, T., Hay, J., Isla, F., Marzeion, B., Meyssignac, B., and Sebesvari, Z.: Sea Level Rise and
680 Implications for Low Lying Islands, Coasts and Communities., 355, 2019.

681 Passaro, M., Cipollini, P., Vignudelli, S., Quartly, G. D., and Snaith, H. M.: ALES: A multi-mission adaptive subwaveform
682 retracker for coastal and open ocean altimetry, 145, https://doi.org/10.1016/j.rse.2014.02.008, 2014.

683 Passaro, M., Cipollini, P., and Benveniste, J.: Annual sea level variability of the coastal ocean: The Baltic Sea-North Sea
684 transition zone, 120, https://doi.org/10.1002/2014JC010510, 2015.

685 Passaro, M., Dinardo, S., Quartly, G. D., Snaith, H. M., Benveniste, J., Cipollini, P., and Lucas, B.: Cross-calibrating ALES
686 Envisat and CryoSat-2 Delay-Doppler: A coastal altimetry study in the Indonesian Seas, 58,
687 https://doi.org/10.1016/j.asr.2016.04.011, 2016.

688 Passaro, M., Rose, S. K., Andersen, O. B., Boergens, E., Calafat, F. M., Dettmering, D., and Benveniste, J.: ALES+:
689 Adapting a homogenous ocean retracker for satellite altimetry to sea ice leads, coastal and inland waters, 211,
690 https://doi.org/10.1016/j.rse.2018.02.074, 2018.

691 Passaro, M., Müller, F. L., Oelsmann, J., Rautiainen, L., Dettmering, D., Hart-Davis, M. G., Abulaitijiang, A., Andersen, O.
692 B., Høyer, J. L., Madsen, K. S., Ringgaard, I. M., Särkkä, J., Scarrott, R., Schwatke, C., Seitz, F., Tuomi, L., Restano, M.,
693 and Benveniste, J.: Absolute Baltic Sea Level Trends in the Satellite Altimetry Era: A Revisit, 8,
694 https://doi.org/10.3389/fmars.2021.647607, 2021.

695 Picaut, J., Hackert, E., Busalacchi, A. J., Murtugudde, R., and Lagerloef, G. S. E.: Mechanisms of the 1997–1998 El Niño–
696 La Niña, as inferred from space-based observations, 107, https://doi.org/10.1029/2001jc000850, 2002.

697 Raj, R. P., Andersen, O. B., Johannessen, J. A., Gutknecht, B. D., Chatterjee, S., Rose, S. K., Bonaduce, A., Horwath, M.,
698 Ranndal, H., Richter, K., Palanisamy, H., Ludwigsen, C. A., Bertino, L., Nilsen, J. E. Ø., Knudsen, P., Hogg, A., Cazenave,
699 A., and Benveniste, J.: Arctic sea level budget assessment during the grace/argo time period, 12,
700 https://doi.org/10.3390/rs12172837, 2020.

701 Richter, K., Nilsen, J. E. Ø., and Drange, H.: Contributions to sea level variability along the Norwegian coast for 1960-2010,
702 117, https://doi.org/10.1029/2011JC007826, 2012.

703 Richter, K., Meyssignac, B., Slangen, A. B. A., Melet, A., Church, J. A., Fettweis, X., Marzeion, B., Agosta, C., Ligtenberg,
704 S. R. M., Spada, G., Palmer, M. D., Roberts, C. D., and Champollion, N.: Detecting a forced signal in satellite-era sea-level
705 change, 15, https://doi.org/10.1088/1748-9326/ab986e, 2020.

706 Röhrs, J., Sperrevik, A. K., and Christensen, K. H.: NorShelf: A reanalysis and data-assimilative forecast model for the
707 Norwegian Shelf Sea, 2018.

708 Rose, S. K., Andersen, O. B., Passaro, M., Ludwigsen, C. A., and Schwatke, C.: Arctic ocean sea level record from the
709 complete radar altimetry era: 1991-2018, 11, https://doi.org/10.3390/rs11141672, 2019.

710 von Schuckmann, K., le Traon, P. Y., Smith, N., Pascual, A., Brasseur, P., Fennel, K., Djavidnia, S., Aaboe, S., Fanjul, E.
711 A., Autret, E., Axell, L., Aznar, R., Benincasa, M., Bentamy, A., Boberg, F., Bourdallé-Badie, R., Nardelli, B. B., Brando,
712 V. E., Bricaud, C., Breivik, L. A., Brewin, R. J. W., Capet, A., Ceschin, A., Ciliberti, S., Cossarini, G., de Alfonso, M., de
713 Pascual Collar, A., de Kloe, J., Deshayes, J., Desportes, C., Drévillon, M., Drillet, Y., Droghei, R., Dubois, C., Embury, O.,
714 Etienne, H., Fratianni, C., Lafuente, J. G., Sotillo, M. G., Garric, G., Gasparin, F., Gerin, R., Good, S., Gourrion, J.,
715 Grégoire, M., Greiner, E., Guinehut, S., Gutknecht, E., Hernandez, F., Hernandez, O., Høyer, J., Jackson, L., Jandt, S., Josey,
716 S., Juza, M., Kennedy, J., Kokkini, Z., Korres, G., Kõuts, M., Lagemaa, P., Lavergne, T., le Cann, B., Legeais, J. F.,
717 Lemieux-Dudon, B., Levier, B., Lien, V., Maljutenko, I., Manzano, F., Marcos, M., Marinova, V., Masina, S., Mauri, E.,
718 Mayer, M., Melet, A., Mélin, F., Meyssignac, B., Monier, M., Müller, M., Mulet, S., Naranjo, C., Notarstefano, G.,
719 Paulmier, A., Gomez, B. P., Pérez Gonzalez, I., Peneva, E., Perruche, C., Peterson, K. A., Pinardi, N., Pisano, A., Pardo, S.,
720 Poulain, P. M., Raj, R. P., Raudsepp, U., Ravdas, M., Reid, R., Rio, M. H., Salon, S., Samuelsen, A., Sammartino, M., et al.:
721 Copernicus Marine Service Ocean State Report, 11, https://doi.org/10.1080/1755876X.2018.1489208, 2018.

722 Siegismund, F., Johannessen, J., Drange, H., Mork, K. A., and Korablev, A.: Steric height variability in the Nordic Seas,
723 112, https://doi.org/10.1029/2007JC004221, 2007.

724 Simpson, M. J. R., Nilsen, J. E. Ø., Ravndal, O. R., Breili, K., Sande, H., Kierulf, H. P., Steffen, H., Jansen, E., Carson, M.,
725 and Vestøl, O.: Sea Level Change for Norway Past and Present Observations and Projections to 2100, 1–156 pp., 2015.

726 Simpson, M. J. R., Ravndal, O. R., Sande, H., Nilsen, J. E. Ø., Kierulf, H. P., Vestøl, O., and Steffen, H.: Projected 21st
727 century sea-level changes, observed sea level extremes, and sea level allowances for Norway, 5,
728 https://doi.org/10.3390/jmse5030036, 2017.

729 Volkov, D. L. and Pujol, M. I.: Quality assessment of a satellite altimetry data product in the Nordic, Barents, and Kara seas,
730 117, https://doi.org/10.1029/2011JC007557, 2012.

731 Woodworth, P. L.: A note on the nodal tide in sea level records, https://doi.org/10.2112/JCOASTRES-D-11A-00023.1,
732 2012.

733 Xu, X.-Y., Xu, K., Xu, Y., and Shi, L.-W.: Coastal Altimetry: A Promising Technology for the Coastal Oceanography
734 Community, in: Estuaries and Coastal Zones - Dynamics and Response to Environmental Changes, 1–19,
735 https://doi.org/10.5772/intechopen.89373, 2019.

736 Zhang, Z., Lu, Y., and Hsu, H.: Detecting ocean currents from satellite altimetry, satellite gravity and ocean data, in:

737 International Association of Geodesy Symposia, https://doi.org/10.1007/978-3-540-49350-1_3, 2007.

738

739
740